Original Article

PROSTATE INTERNATIONAL

Prostate Int 2014;2(4):188-195 • http://dx.doi.org/10.12954/PI.14067

# Feasibility of multiparametric prostate magnetic resonance imaging in the detection of cancer distribution: histopathological correlation with prostatectomy specimens

Kosuke Kitamura[1,2], Satoru Muto[1], Isao Yokota[3], Kazutane Hoshimoto[4], Tatsuro Kaminaga[5], Takahiro Noguchi[1], Syou-Ichiro Sugiura[1], Hisamitsu Ide[1], Raizo Yamaguchi[1], Shigeru Furui[5], Shigeo Horie[2]

[1]*Department of Urology, Teikyo University School of Medicine, Tokyo, Japan*
[2]*Department of Urology, Juntendo University, Graduate School of Medicine, Tokyo, Japan*
[3]*School of Integrated Health Science, Faculty of Medicine, The University of Tokyo, Tokyo, Japan*
*Departments of* [4]*Pathology and* [5]*Radiology, Teikyo University School of Medicine, Tokyo, Japan*

**Purpose:** To prevent overtreatment, it is very important to diagnose the precise distribution and characteristics of all cancer lesions, including small daughter tumors. The purpose of this study was to evaluate the efficacy of T2-weighted magnetic resonance imaging (T2W), diffusion-weighted magnetic resonance imaging (DWI), magnetic resonance spectroscopy ($^1$H-MRS), and prostate biopsy (PBx) in the detection of intraprostatic cancer distribution.

**Methods:** All patients underwent T2W, DWI, $^1$H-MRS, and PBx followed by radical prostatectomy (RP). Individual prostates were divided into 12 segmental regions, each of which was examined for the presence or absence of malignancy on the basis of T2W, DWI, $^1$H-MRS, and PBx, respectively. These results were compared with the histopathological findings for RP specimens.

**Results:** We included 54 consecutive patients with biopsy-proven prostate cancer (mean age, 62.7 years; median prostate-specific antigen level, 5.7 ng/mL) in this study. We could detect cancer in 247 of 540 evaluable lesions. The area under the receiver operator characteristic curve analysis yielded a higher value for DWI (0.68) than for T2W (0.65), $^1$H-MRS (0.54), or PBx (0.56). In 180 cancerous regions of RP specimens with false-negative PBx results, T2W+DWI had the highest positive rate (53.3%) compared with that of each sequence alone, including T2W (45.6%), DWI (41.1%), and $^1$H-MRS (30.0%).

**Conclusions:** Multiparametric magnetic resonance imaging (T2W, $^1$H-MRS, DWI) enables the detection of prostate cancer distribution with reasonable sensitivity and specificity. T2W+DWI was particularly effective in detecting cancer distribution with false-negative PBx results.

**Keywords:** Prostate neoplasms, Magnetic resonance imaging, Diffusion magnetic resonance imaging, Magnetic resonance spectroscopy

## INTRODUCTION

Prostate cancer (PCa) is a major disease affecting men worldwide, and the detection of malignancy at an early stage is essential to treatment [1,2]. In Cancer of the Prostate Strategic Urologic Research Endeavor, the proportion of patients with low-risk disease has increased, and conversely, high-risk diagnoses have decreased [3]. The current methods of PCa detec-

**Corresponding author:** Satoru Muto
Department of Urology, Teikyo University School of Medicine, 2-11-1, Kaga, Itabashi-ku, Tokyo 173-8605, Japan
E-mail: muto@med.teikyo-u.ac.jp / Tel: +81-3-3964-2497 / Fax: +81-3-3964-8934
Submitted: 11 November 2014 / Accepted after revision: 19 November 2014



http://p-international.org/
pISSN: 2287-8882 • eISSN: 2287-903X

tion include digital rectal examination, serum concentration of prostate-specific antigen (PSA), and transrectal ultrasonography-guided prostate biopsy (PBx), but these are of limited accuracy for the majority of early cancers. To prevent overtreatment [4], the most important goal is to diagnose the precise distribution and characteristics of all cancer lesions, including small daughter tumors. As a noninvasive tool, magnetic resonance imaging (MRI) plays an increasingly important role in the detection, localization, and staging of PCa [5-8]. Although T2-weighted magnetic resonance imaging (T2W) has been the mainstay of prostate MRI, it is generally acknowledged to be nonspecific for cancer, because low-signal-intensity lesions in the peripheral zone (Pz) can result from prostatitis, scarring, or hyperplasia [9]. Diffusion-weighted MRI (DWI) can offer valuable information about the microstructure and pathophysiology of tissues based on the diffusion properties of the water molecules [8,10-13]. MR spectroscopy ($^1$H-MRS) has the ability to provide chemical information about metabolites in normal and abnormal tissues. The purpose of this study was to evaluate the efficacy of T2W, DWI, $^1$H-MRS, and PBx in the detection of intraprostatic cancer distribution.

## MATERIALS AND METHODS

### 1. Patients

Between February 2009 and July 2013, patients with cT1c-T2N0M0 biopsy-proven localized PCa who underwent T2W, DWI, $^1$H-MRS, and PBx followed by radical prostatectomy (RP), and who did not receive neoadjuvant hormonal therapy, were included in this study. Patients with a PSA value above 2.5 ng/mL underwent T2W and DWI, followed by PBx. We previously demonstrated that MRS had no effect on PBx [14]. Therefore, we performed $^1$H-MRS after PBx, followed by RP. Full data included age; preoperative PSA values; MRI data including T2W, DWI, and $^1$H-MRS; and PBx pathological results. TNM classification was based on guidelines set forth in the Union for International Cancer Control, 7th edition [15]. The present study was carried out in accordance with the protocol and in compliance with the moral, ethical, and scientific principles governing clinical research as set forth in the Declaration of Helsinki (1989).

### 2. MRI procedures

All examinations were performed by using a 1.5-Tesla MRI system (Signa LX Horizon Echospeed, General Electric Medical Systems Inc., Buckinghamshire, UK). T2W images of the prostate and seminal vesicle included the following parameters: repetition time (TR), 3,300–4,000 ms; echo time (TE), 80–100 ms; slice thickness, 3.0 mm; gap, 0.3 mm; and matrix, 260×256. DWI images of the prostate and seminal vesicle included the following parameters: TR, 3,300–5,000 ms; TE, 74–76 ms; slice thickness, 4.0 mm; gap, 0.3–0.4 mm; and matrix, 88×128.

The following sequence and imaging conditions were used: sequence=point-resolved spectroscopy based 3D PROSE (PROstate spectroscopy imaging exam); TR/TE=2,000/130 ms; spectral width=1,250 Hz; data acquisition points=256; activation area=8.0 or 16.0 cm$^2$; encode=8×8 or 16×16; and number of excitations=2. A body coil was used for radio frequency transmission, whereas the receiver coil was an endorectal coil (BPX-10; Nihon Medrad K.K., Tokyo, Japan) placed on the anterior surface of the rectum in close contact with the posterior aspect of the prostate. Spectral data correcting the volume of interest (VOI) were manually set on the axial localization image to cover the entire outer gland. VOI thickness was 2.0 cm. Six planes of very selective suppression radio frequency pulses were set at a region adjacent to a VOI. Full width at half maximum of water peak after shimming was less than 14 Hz in all participants. The $^1$H-MRS data were processed by using the software supplied (SAGE II, General Electric Medical Systems) on the MRI console. Each spectral signal was zero-filled to 512 points and multiplied by 2 Hz of exponential function. Fourier transformation, phase adjustment, frequency adjustment, baseline correction, and calculation of the CCr ratio (choline+creatine/citrate ratio) were carried out automatically. The peak areas of citrate (at 2.8 ppm), choline (at 3.2 ppm), and creatine (at 3.0 ppm) were measured. A CCr ratio ≥1.07 indicated the existence of cancer, as we reported previously [14]. On the basis of data from the 20 patients with localized PCa who underwent RP, we decided that the cutoff value for PCa diagnosis by $^1$H-MRS would be ≥1.07, which is equivalent to the mean+2 standard deviations of the CCr ratio for a normal (noncancerous) Pz at Teikyo University, Tokyo, Japan [14].

MRI data sets were prospectively evaluated by a radiologist (TK, with 28 years' accumulated experience in prostate MRI) and two urologists (K.K. and S.M., with 10 and 22 years' accumulated experience in prostate MRI, respectively). MRI data sets were assessed in consensus and reviewers were aware that patients had biopsy-proven PCa, but they were blinded to the initial PSA values and PBx results as well as to histopathologic findings. MR images were evaluated; the criterion for cancer presence was a mass or nodule with homogenously low signal intensity showing ill-defined margins on T2W (Fig. 1B) [16] and appearing hyper-intense on DWI (Fig. 1C) [5,7,17]. $^1$H-MRS images were evaluated; the criterion for cancer pres-

ence was indicated regions in which the CCr ratio was ≥1.07 as mentioned above (Fig. 1D) [14].

### 3. Histopathological analysis

PBx was performed as transrectal and transperineal biopsy under ultrasound guidance. Transrectal biopsy included 10 regions of the Pz and transitional zone (Tz) of the middle gland. Transperineal biopsy included 2 regions of the apex gland. RP specimens were sliced into 5 mm-thick horizontal sections perpendicular to the dorsal surface of the urethral mucosa. The strip preparations were fixed in formalin and stained with hematoxylin-eosin. The pathological diagnoses were made by a single pathologist (K.H.). Sections were assessed for the presence of tumor and the Gleason score of individual foci of PCa. The grids used for mapping were similar to those used for MRI evaluation to allow for correlation of radiologic findings and pathologic findings.

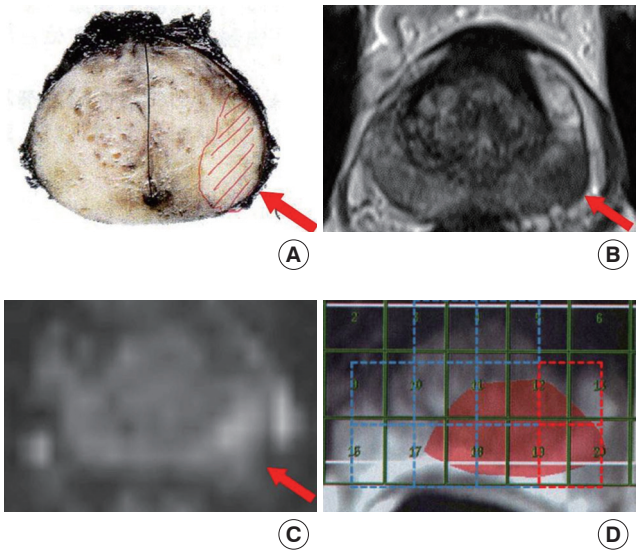


**Fig. 1.** Prostate cancer (PCa) in a 68-year-old man with an initial prostate-specific antigen value of 14 ng/mL. (A) Radical prostatectomy (RP) specimen: histopathologic findings at the peripheral zone at the midprostate level indicate tumor presence (Gleason score, 4+3); the diagonal red lines indicate the presence of PCa on the basis of histopathological findings. The remaining panels (B–D) correspond to the slices of the RP specimen. (B) Axial T2-weighted magnetic resonance imaging (T2W) image demonstrating a mass of homogeneously low signal intensity with ill-defined margins (red arrow). (C) Diffusion-weighted magnetic resonance imaging image demonstrates a mass of hyper-signal intensity (red arrow). (D) Magnetic resonance spectroscopy imaging shows abnormal metabolism characterized by high choline and low citrate peaks in the region of the T2W abnormality (red area). Red dotted-line boxes indicate the regions suggestive of malignancy. Blue dotted-line boxes indicate the normal findings suggestive of benign regions.

### 4. Analysis of data set

For tumor localization, a prostate was divided into halves: right (R) and left (L). Then each half was divided into 6 segments: outside Pz anterior, outside Pz posterior, inside Pz, central Tz, Tz anterior, and apex. Thus, in each case, we had 12 segmental regions of interest (ROIs) within the whole prostate of each patient (Fig. 2). PBx specimens for each segmental region were evaluated for cancer presence. To evaluate the diagnostic performance of each MR sequence (Fig. 2), the sensitivity, specificity, positive predictive value (PPV), and negative predictive value (NPV) of T2W, DWI, $^{1}$H-MRS, and PBx were compared between groups by using the Z-test. For this approach, the sensitivity of an imaging modality or PBx result was defined as the probability of correctly identifying a histopathologically proven cancer focus. Specificity was defined as the probability of correctly identifying regions negative for cancer. In addition, we evaluated the combined diagnostic accuracy of multiple imaging variables. We calculated areas under the receiver operator curves (AUCs) of each MR sequence and PBx. An region of Interest study was performed by using Discover JMP ver. 11.0 (SAS Institute Inc., Cary, NC, USA). Variables are expressed as medians with interquartile ranges (IQRs). All *P*-values corresponded to two-sided tests, with a *P*-value of 0.05 considered to represent a significant difference.

## RESULTS

### 1. Patients and pathological data

In this study, 54 consecutive patients who underwent RP for PCa were evaluated. The characteristics of the patients are shown in Table 1. The mean age of the patients was 62.7 years, and the patients' median initial PSA level was 5.7 ng/mL (IQR, 4.4–7.6 ng/mL). The median intervals between T2W with DWI and PBx, PBx and $^{1}$H-MRS, and $^{1}$H-MRS and RP were 15.5, 75.0, and 71.0 days, respectively. Tumor staging was as follows: 33.3% were cT1c (n=18) and 66.7% were cT2 (n=36). Further-

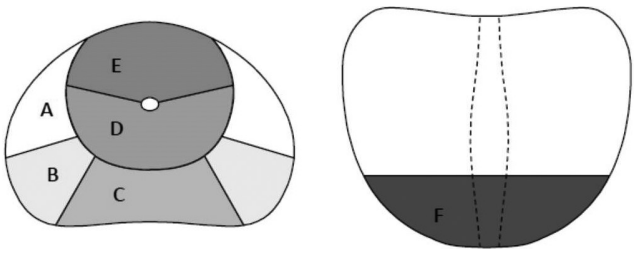


**Fig. 2.** Each prostate was divided into 12 segmented regions. For tumor localization, each prostate was divided into halves: right and left. Each half was further divided into 6 regions as follows: (A) outside peripheral zone (Pz) anterior, (B) outside Pz posterior, (C) inside Pz, (D) central transitional zone (Tz), (E) Tz anterior, (F) apex.


http://dx.doi.org/10.12954/PI.14067

**Table 1.** Characteristics of the patients (n=54)

| Characteristic | Value |
|---|---|
| Age (yr), mean±SD | 62.7±6.4 |
| Baseline PSA (ng/mL) | 5.7 (4.4–7.6) |
| Interval between T2W with DWI and PBx (day) | 15.5 (24.8–54.5) |
| Interval between PBx and $^{1}$H-MRS (day) | 75.0 (39.0–107.0) |
| Interval between $^{1}$H-MRS and prostatectomy (day) | 71.0 (34.5–114.3) |
| cT | |
| cT1c | 18 (33.3) |
| cT2 | 36 (66.7) |
| pT | |
| pT2a | 17 (31.5) |
| pT2b | 2 (3.7) |
| pT2c | 24 (44.4) |
| pT3a | 7 (13.0) |
| pT3b | 4 (7.4) |
| Gleason score | |
| 3+3 | 17 (31.5) |
| 3+4 | 11 (20.4) |
| 4+3 | 17 (31.5) |
| ≥4+4 | 9 (16.6) |

Values are presented as median (interquartile range) or number (%) unless otherwise indicated.
SD, standard deviation; PSA, prostate-specific antigen; T2W, T2-weighted magnetic resonance imaging; DWI, diffusion-weighted magnetic resonance imaging; PBx, prostate biopsy; $^{1}$H-MRS, magnetic resonance spectroscopy.

more, tumors in 43 patients (79.6%) were staged as pT2N0M0, whereas those in 11 patients (20.4%) were staged as pT3N0M0 at the pathologic analysis. No regional lymph node involvement or distant metastases were detected in any of the patients. RP specimens showed 17 patients (31.5%) with GS 3+3, 11 patients (20.4%) with GS 3+4, 17 patients (31.5%) with GS 4+3, 8 patients (14.8%) with GS 4+4, and 1 patient (1.8%) with GS 4+5. In addition, 23 patients (42.6%) had a positive surgical margin.

Of the total number of 540 ROIs, cancer was detected in 174 regions (32.2%) in T2W, in 130 regions (24.1%) in DWI, in 133 regions (24.6%) in $^{1}$H-MRS, in 109 regions (20.2%) in PBx, and in 247 regions (45.7%) in RP specimens.

## 2. Comparison with each MR sequence alone

The power of cancer detection by each sequence was investigated by comparing the sensitivity, specificity, PPV, and NPV (Fig. 3A). PBx had the lowest sensitivity (27.1%). That is, PBx had a high false-negative rate. Sensitivity for T2W was higher than it was for DWI or $^{1}$H-MRS, and specificity for T2W was lower than it was for DWI or $^{1}$H-MRS for all regions. DWI had the highest specificity (92.8%), PPV (83.8%), and NPV (66.3%) in each sequence alone. AUC analysis showed that DWI had a higher AUC (0.68) than did T2W (0.65), $^{1}$H-MRS (0.54), or PBx (0.56) (Fig. 3A). The results of the ROC analysis for T2W, DWI, $^{1}$H-MRS, and PBx are shown in Fig. 4. In the ROC analysis, DWI had the best accuracy for detecting the cancer distribution in each sequence alone. Of 247 cancerous regions in RP specimens, 180 could not be diagnosed by PBx. In 180 cancerous regions of RP specimens with negative PBx results, we compared the positive rates of each sequence alone. T2W had the highest positive rate (45.6%) compared with DWI (41.1%) and $^{1}$H-MRS (30.0%) (Fig. 5).

Fig. 3B shows the diagnostic accuracy only in segmental regions of the Pz. Sensitivity was higher in segmental regions of the Pz, regardless of MRI modality or PBx, than in other segmental regions, whereas specificity and NPV were lower. As was the case in all segmental regions, DWI had the highest AUC in each sequence alone.

### 1) Multiparametric MRI

The diagnostic accuracy of multiparametric MRI (by combining MRI modalities) is shown in Fig. 3A. We evaluated the results of T2W+DWI, T2W+$^{1}$H-MRS, and T2W+DWI+$^{1}$H-MRS, respectively. Compared with MRI sequences alone, multiparametric MRI had higher sensitivity. That is, multiparametric MRI could decrease the false-negative rate. On the other hand, in view of the results that multi-parametric MRI could decrease specificity compared with each sequence alone, multi-parametric MRI was not effective in decreasing the false-positive rate. With the exclusion of $^{1}$H-MRS, there were no obvious differences in the AUC between T2W alone, DWI alone, and multiparametric MRI. In 180 cancerous regions of RP specimens with negative PBx results, T2W+DWI had the highest positive rate (53.3%) compared with each sequence alone (Fig. 5).

### 2) Malignant potential

Among all 540 regions in the RP specimens, we detected 247 cancerous regions (45.7%). Their Gleason scores were as follows: 111 regions (44.9%) had a Gleason 3+3, 56 regions (22.7%) had a Gleason 3+4, 47 regions (19.0%) had a Gleason 4+3, and 29 regions (11.7%) had a Gleason 4+4. The positive rate of each sequence alone by Gleason score is shown in Fig. 6. The positive rate of Gleason 3+3 specimens was almost 30% in all modalities. There was little difference in the positive rate of any Gleason score. In contrast, MR modality tended to show an increase in the positive rate with increasing Gleason score. Notably, the positive rates of DWI (62.1%) and T2W (69.0%) in Gleason 4+4 regions were over 60%.

# DISCUSSION

It is well known that precise diagnosis faces real limitations

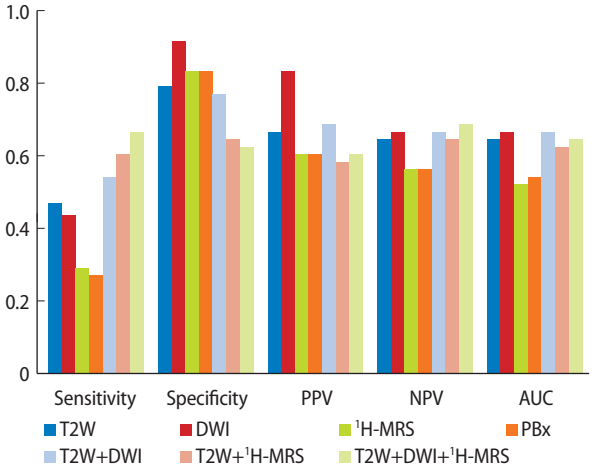


| | Sensitivity | Specificity | PPV | NPV | AUC |
|---|---|---|---|---|---|
| T2W | 0.48 | 0.81 | 0.68 | 0.65 | 0.65 |
| DWI | 0.44 | 0.93 | 0.84 | 0.66 | 0.68 |
| $^{1}$H-MRS | 0.29 | 0.86 | 0.62 | 0.58 | 0.54 |
| PBx | 0.27 | 0.86 | 0.62 | 0.58 | 0.56 |
| T2W+DWI | 0.56 | 0.79 | 0.69 | 0.68 | 0.68 |
| T2W+$^{1}$H-MRS | 0.62 | 0.65 | 0.60 | 0.67 | 0.63 |
| T2W+DWI+$^{1}$H-MRS | 0.68 | 0.63 | 0.61 | 0.70 | 0.66 |

A

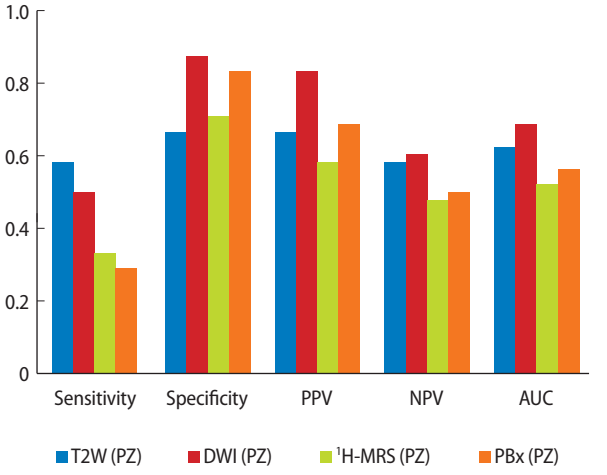


| | Sensitivity | Specificity | PPV | NPV | AUC |
|---|---|---|---|---|---|
| T2W | 0.60 | 0.67 | 0.68 | 0.59 | 0.64 |
| DWI | 0.51 | 0.89 | 0.84 | 0.61 | 0.70 |
| $^{1}$H-MRS | 0.33 | 0.72 | 0.58 | 0.48 | 0.53 |
| PBx | 0.30 | 0.85 | 0.70 | 0.51 | 0.58 |

B

**Fig. 3.** Diagnostic accuracy. (A) The diagnostic accuracy of each sequence alone and multiparametric magnetic resonance imaging (MRI) in all segmental regions. (B) The diagnostic accuracy only in segmental regions of peripheral zone (Pz). PPV, positive predictive value; NPV, negative predictive value; AUC, areas under the receiver operator curve; T2W, T2-weighted MRI; DWI, diffusion-weighted magnetic resonance imaging; $^{1}$H-MRS, magnetic resonance spectroscopy; PBx, prostate biopsy.

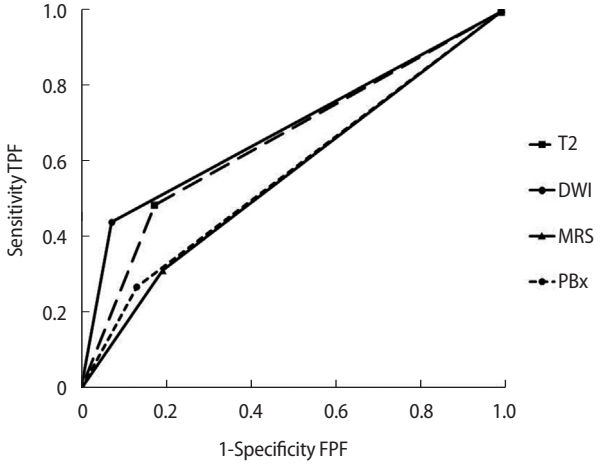


**Fig. 4.** Results of the region of Interest analysis for T2-weighted magnetic resonance imaging (T2W), diffusion-weighted magnetic resonance imaging (DWI), magnetic resonance spectroscopy ($^{1}$H-MRS), and prostate biopsy (PBx). Area under the receiver operator characteristic curve (AUC) analysis found that DWI had a higher AUC of 0.68 compared with T2W (0.65), $^{1}$H-MRS (0.54), and PBx (0.56). TPF, true positive fraction; FPF, false positive fraction.

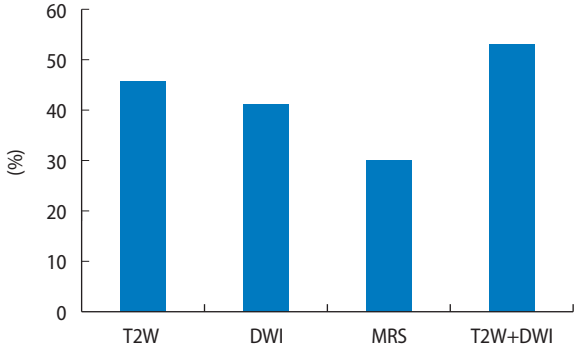


**Fig. 5.** Of 247 cancerous regions in radical prostatectomy (RP) specimens, 180 could not be diagnosed by prostate biopsy (PBx). In 180 cancerous regions of RP specimens with negative PBx results, T2-weighted magnetic resonance imaging (T2W)+diffusion-weighted magnetic resonance imaging (DWI) had the highest positive rate (53.3%) compared with T2W alone (45.6%), DWI alone (41.1%), and magnetic resonance spectroscopy ($^{1}$H-MRS) alone (30.0%).

with digital rectal examination, serum PSA, diagnostic imaging, and PBx [18]. MRI has already been established as a non-invasive diagnostic tool [19]. However, the ideal MRI sequence modality combination has yet to be established.

In our study, DWI had the highest specificity, PPV, NPV, and AUC to detect the presence or absence of PCa in intraprostatic segmental regions (Fig. 3A). We could obtain similar analytical results only in Pz regions. It was reported that DWI provides an important quantitative biophysical parameter that can be


http://dx.doi.org/10.12954/PI.14067

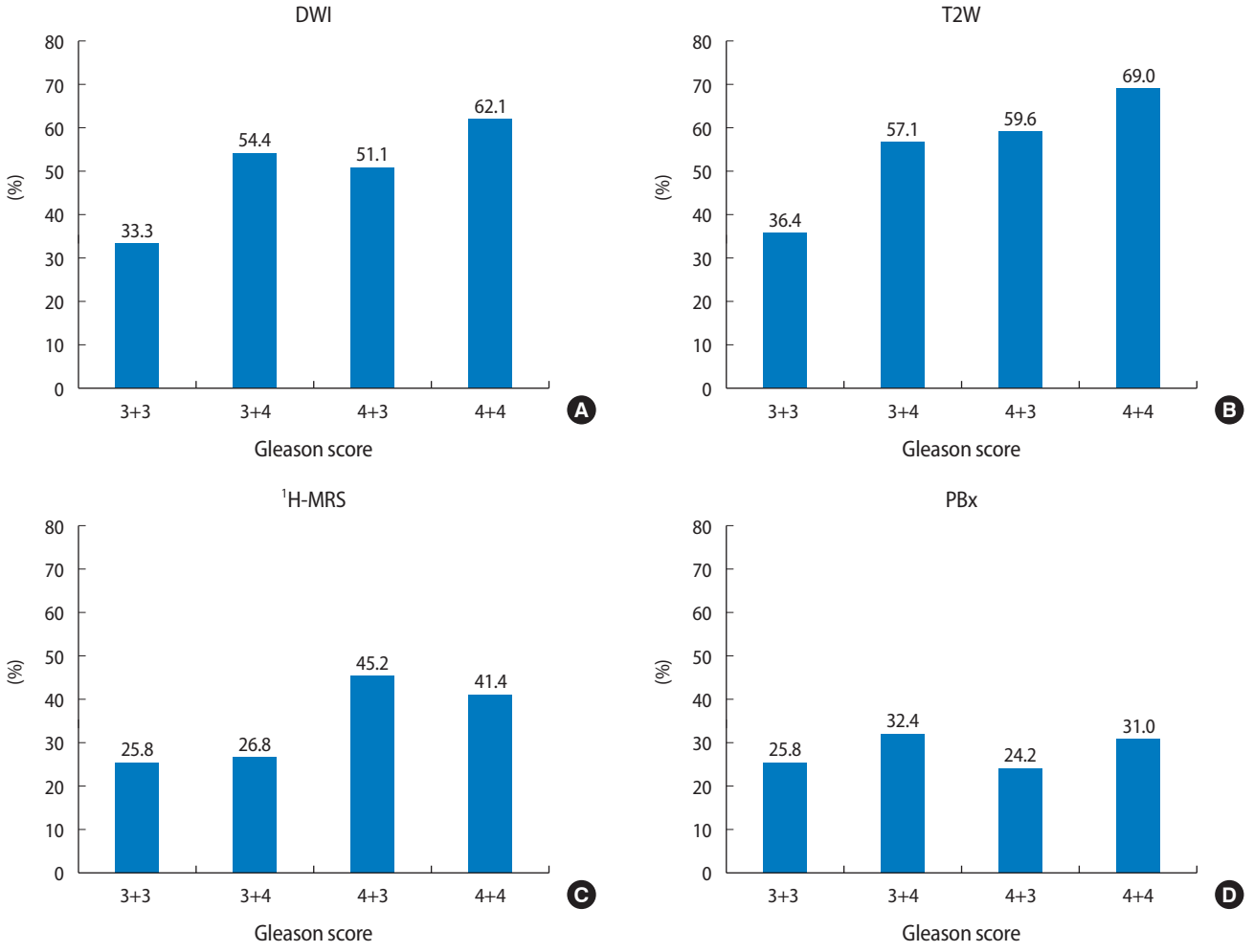


**Fig. 6.** The positive rate of each sequence alone by Gleason score. The positive rate of diffusion-weighted magnetic resonance imaging (DWI; A) and T2-weighted magnetic resonance imaging (T2W; B) increased with increasing Gleason score. In contrast, regardless of Gleason score, the positive rate of prostate biopsy (PBx; D) remained cons istently low. $^{1}$H-MRS, magnetic resonance spectroscopy.

used to differentiate benign from malignant prostate tissue [20]. In the European Society of Urogenital Radiology (ESUR) prostate MR guidelines (2012) [5], DWI is noted to be a powerful clinical tool, as it allows apparent diffusion coefficient (ADC) maps to be calculated, enabling qualitative and quantitative assessment of PCa aggressiveness. Even though we did not use an ADC map in this study, DWI had the best outcome among the MRI modalities.

The ESUR prostate MR guidelines (2012) reported that T2W alone is sensitive but not specific for PCa and should be improved by using two other functional techniques [5,21]. Turkbey et al. [9] reported that sensitivity for T2W was significantly higher than it was for dynamic contrast-enhanced MRI or $^{1}$H-MRS, and that specificity for T2W was lower than it was for dynamic contrast-enhanced MRI or $^{1}$H-MRS ($P<0.001$) for all regions. Our data also demonstrated that, although T2W alone had the best sensitivity (48.2%), T2W alone had the worst specificity (81.2%) in each sequence (Fig. 3A). As a result, T2W (0.65) had a lower AUC than did DWI (0.68) (Fig. 3A). Therefore, although it had insufficient diagnostic capacity, T2W was absolutely imperative for detecting cancer distribution on its own.

On the other hand, $^{1}$H-MRS and PBx had low accuracy in detecting PCa localization. $^{1}$H-MRS uses metabolic information and makes biochemical quantitation at specific regions of the prostate possible in a noninvasive manner [22]. The ratio of the sum of the citrate and choline peaks to the citrate peak can differentiate PCa from normal parenchyma [5,14, 23-25]. In this study, however, as in our previous report [22], $^{1}$H-MRS alone and multi-parametric MRI using $^{1}$H-MRS had a relatively lower AUC. This was especially the case due to the obvious low sensitivity of $^{1}$H-MRS compared with T2W or DWI. $^{1}$H-MRS can provide valuable information about lesion aggression but requires expertise.

It was previously reported that the standard PBx is poor at sampling cancers, leading to the underdiagnosis of clinically significant disease [26]. Sampling accuracy tends to decrease progressively when the prostate increases in size, not only due to the larger volume itself, but also because of the more dispersed and thin distribution of the Pz tissue owing to Tz enlargement [27]. In this study, compared with each MRI sequence, PBx had relatively low sensitivity and specificity in detecting PCa localization. In addition, compared with MRI, we believe the most critical problem is that PBx is an invasive procedure.

Recently, the usefulness of multiparametric MRI has been widely reported. Most of these authors concluded that multiparametric MRI is the best imaging sequence for the detection of PCa [17,28]. In our study, although T2W+DWI+$^{1}$H-MRS showed the best sensitivity, no multiparametric MRI could surpass the AUC value of DWI alone (Fig. 3A). On the other hand, as shown in Fig. 5, in 180 cancerous regions of RP specimens with negative PBx results, T2W+DWI had a higher positive rate (53.3%) than any sequence alone, including T2W (45.6%), DWI (41.1%), and $^{1}$H-MRS (30.0%) (Fig. 5). Previously, Kim et al. [27] concluded that adjunct use of DWI with T2W could increase performance compared with T2W alone. Therefore, judging from the results in this study and previous reports, T2W+DWI is the best combination to detect cancer distribution under the present circumstances, especially in cancerous regions with negative PBx results.

There were several limitations to this study. First, dynamic contrast-enhanced MRI, which has shown promise in several investigations, was not evaluated in the current study. Ocak et al. [28] reported improvement in specificity by combining T2W with dynamic contrast-enhanced MRI. We intend to incorporate dynamic contrast-enhanced MRI in the next cohort of patients studied. Second, we could not completely avoid the deformation and shrinkage of RP specimens after fixation, or errors in the sectioning angle. Although the issue of misregistration has been approached in various ways [9], it is very difficult to correlate imaging findings with histopathologic findings.

In conclusion, we could show the efficacy and limitations of multiparametric MRI, including the findings that anatomic (T2W) and functional (dynamic contrast-enhanced MRI and $^{1}$H-MRS) modalities increase the performance of MRI in detecting cancer distribution.

## CONFLICT OF INTEREST

No potential conflict of interest relevant to this article was reported.

## REFERENCES


1. Turkbey B, Albert PS, Kurdziel K, Choyke PL. Imaging localized prostate cancer: current approaches and new developments. AJR Am J Roentgenol 2009;192:1471-80.
2. Kumar V, Jagannathan NR, Thulkar S, Kumar R. Prebiopsy magnetic resonance spectroscopy and imaging in the diagnosis of prostate cancer. Int J Urol 2012;19:602-13.
3. Barocas DA, Chen V, Cooperberg M, Goodman M, Graff JJ, Greenfield S, et al. Using a population-based observational cohort study to address difficult comparative effectiveness research questions: the CEASAR study. J Comp Eff Res 2013;2:445-60.
4. Hashimoto Y, Okamoto A, Imai A, Yoneyama T, Hatakeyama S, Yoneyama T, et al. Biochemical outcome of small-volume or insignificant prostate cancer treated with radical prostatectomy in Japanese population. Int J Clin Oncol 2012;17:119-23.
5. Barentsz JO, Richenberg J, Clements R, Choyke P, Verma S, Villeirs G, et al. ESUR prostate MR guidelines 2012. Eur Radiol 2012;22:746-57.
6. Aydin H, Kizilgoz V, Tatar IG, Damar C, Ugan AR, Paker I, et al. Detection of prostate cancer with magnetic resonance imaging: optimization of T1-weighted, T2-weighted, dynamic-enhanced T1-weighted, diffusion-weighted imaging apparent diffusion coefficient mapping sequences and MR spectroscopy, correlated with biopsy and histopathological findings. J Comput Assist Tomogr 2012;36:30-45.
7. Kitajima K, Kaji Y, Fukabori Y, Yoshida K, Suganuma N, Sugimura K, et al. Prostate cancer detection with 3 T MRI: comparison of diffusion-weighted imaging and dynamic contrast-enhanced MRI in combination with T2-weighted imaging. J Magn Reson Imaging 2010;31:625-31.
8. Doo KW, Sung DJ, Park BJ, Kim MJ, Cho SB, Oh YW, et al. Detectability of low and intermediate or high risk prostate cancer with combined T2-weighted and diffusion-weighted MRI. Eur Radiol 2012;22:1812-9.
9. Turkbey B, Pinto PA, Mani H, Bernardo M, Pang Y, McKinney YL, et al. Prostate cancer: value of multiparametric MR imaging at 3 T for detection--histopathologic correlation. Radiology 2010;255:89-99.
10. Li B, Cai W, Lv D, Guo X, Zhang J, Wang X, et al. Comparison of MRS and DWI in the diagnosis of prostate cancer based on sextant analysis. J Magn Reson Imaging 2013;37:194-200.
11. Zelhof B, Pickles M, Liney G, Gibbs P, Rodrigues G, Kraus S, et al. Correlation of diffusion-weighted magnetic resonance data with cellularity in prostate cancer. BJU Int 2009;103:883-8.
12. Quentin M, Schimmoller L, Arsov C, Rabenalt R, Antoch G, Albers P, et al. Increased signal intensity of prostate lesions



http://dx.doi.org/10.12954/PI.14067

on high b-value diffusion-weighted images as a predictive sign of malignancy. Eur Radiol 2014;24:209-13.
13. Shigemura K, Yamanaka N, Yamashita M. Can diffusion-weighted magnetic resonance imaging predict a high Gleason score of prostate cancer? Korean J Urol 2013;54:234-8.
14. Saito K, Kaminaga T, Muto S, Ide H, Nishio K, Kamiyama Y, et al. Clinical efficacy of proton magnetic resonance spectroscopy (1H-MRS) in the diagnosis of localized prostate cancer. Anticancer Res 2008;28(3B):1899-904.
15. Sobin LH, Gospodarowicz MK, Wittekind CH; International Union against Cancer. TNM classification of malignant tumors. 7th ed. Chichester: Wiley-Blackwell; 2009.
16. Heijmink SW, Futterer JJ, Hambrock T, Takahashi S, Scheenen TW, Huisman HJ, et al. Prostate cancer: body-array versus endorectal coil MR imaging at 3 T-comparison of image quality, localization, and staging performance. Radiology 2007; 244:184-95.
17. Shukla-Dave A, Hricak H. Role of MRI in prostate cancer detection. NMR Biomed 2014;27:16-24.
18. Blomqvist L, Carlsson S, Gjertsson P, Heintz E, Hultcrantz M, Mejare I, et al. Limited evidence for the use of imaging to detect prostate cancer: a systematic review. Eur J Radiol 2014; 83:1601-6.
19. Kumar R, Jagannathan NR. Prebiopsy magnetic resonance studies for prostate cancer diagnosis. Int J Urol 2013;20:140-1.
20. Hosseinzadeh K, Schwarz SD. Endorectal diffusion-weighted imaging in prostate cancer to differentiate malignant and benign peripheral zone tissue. J Magn Reson Imaging 2004;20: 654-61.
21. Wu LM, Xu JR, Ye YQ, Lu Q, Hu JN. The clinical value of diffusion-weighted imaging in combination with T2-weighted imaging in diagnosing prostate carcinoma: a systematic review and meta-analysis. AJR Am J Roentgenol 2012;199:103-10.
22. Panych LP, Roebuck JR, Chen NK, Tang Y, Madore B, Tempany CM, et al. Investigation of the PSF-choice method for reduced lipid contamination in prostate MR spectroscopic imaging. Magn Reson Med 2012;68:1376-82.
23. Mueller-Lisse UG, Scherr MK. Proton MR spectroscopy of the prostate. Eur J Radiol 2007;63:351-60.
24. Nagarajan R, Margolis D, Raman S, Sarma MK, Sheng K, King CR, et al. MR spectroscopic imaging and diffusion-weighted imaging of prostate cancer with Gleason scores. J Magn Reson Imaging 2012;36:697-703.
25. King CR, McNeal JE, Gill H, Presti JC Jr. Extended prostate biopsy scheme improves reliability of Gleason grading: implications for radiotherapy patients. Int J Radiat Oncol Biol Phys 2004;59:386-91.
26. Turkbey B, Choyke PL. Multiparametric MRI and prostate cancer diagnosis and risk stratification. Curr Opin Urol 2012; 22:310-5.
27. Kim CK, Park BK, Lee HM, Kwon GY. Value of diffusion-weighted imaging for the prediction of prostate cancer location at 3T using a phased-array coil: preliminary results. Invest Radiol 2007;42:842-7.
28. Ocak I, Bernardo M, Metzger G, Barrett T, Pinto P, Albert PS, et al. Dynamic contrast-enhanced MRI of prostate cancer at 3 T: a study of pharmacokinetic parameters. AJR Am J Roentgenol 2007;189:849.